Impact of the Sunda Shelf on the Climate of the Maritime Continent

Anta-Clarisse Sarr, Pierre Sepulchre, Laurent Husson

JGR Atmospheres

RESEARCH ARTICLE
10.1029/2018JD029971

Impact of the Sunda Shelf on the Climate of the Maritime Continent

Anta-Clarisse Sarr[1,2], **Pierre Sepulchre**[2], **and Laurent Husson**[1]

[1]ISTerre, University Grenoble Alpes, CNRS, F-38000, Grenoble, France, [2]Laboratoire des Sciences du Climat et de l'Environnement, LSCE/IPSL, CEA-CNRS-UVSQ, Université Paris Saclay, F-91191, Gif-Sur-Yvette, France

Key Points:
- An emerged Sunda shelf induces increased advection and precipitation over the Maritime Continent at seasonal scale
- Seasonal response is not dependent on convection parameterization in the model
- The magnitude of regional climate impact of an emerged shelf only partly depends on the vegetation cover prescribed

Supporting Information:
- Supporting Information S1

Correspondence to:
A.-C. Sarr,
anta-clarisse.sarr@univ-grenoble-alpes.fr

Citation:
Sarr, A.-C., Sepulchre, P., & Husson, L. (2019). Impact of the Sunda shelf on the climate of the Maritime Continent. *Journal of Geophysical Research: Atmospheres*, *124*. https://doi.org/10.1029/2018JD029971

Received 19 NOV 2018
Accepted 6 FEB 2019
Accepted article online 12 FEB 2019

Author Contributions:
Formal analysis: Anta-Clarisse Sarr, Pierre Sepulchre
Methodology: Anta-Clarisse Sarr, Pierre Sepulchre, Laurent Husson
Supervision: Pierre Sepulchre, Laurent Husson
Writing - original draft: Anta-Clarisse Sarr, Pierre Sepulchre, Laurent Husson

Abstract Drastic paleogeography changes in the Indonesian archipelago over the Plio-Pleistocene, either in response to sea level oscillations or vertical land motion, enabled the periodic emergence of the Sunda shelf. When emerged, this wide continental platform in the heart of the Maritime Continent may have modified regional and global climate systems. We investigate the effect of the exposure of the Sunda shelf on climate dynamics using a set of numerical simulations with (i) atmosphere-land surface and (ii) fully coupled general circulation models. We first explore the impact of convection schemes on the rainfall regime simulated over the Maritime Continent and show how they could explain the discrepancies among previous studies. We further depict a robust and common mechanism that prevails. We show that diurnal heating of the surface of the continental platform enhances low-level convergence and local convection, and fosters local precipitations. This effect, to a second order, is modulated by the radiative effect and increased turbulent heat flux driven by vegetated surface properties such as albedo or roughness. Increasing precipitations over the exposed platform also impacts freshwater export into seawater, making salinity of the Indian Ocean and Indonesian Throughflow highly dependent on the routing scheme over the exposed shelf.

1. Introduction

The "Maritime Continent" with its complex physiography made of islands and shallow seas (Figure 1a) is a key part of the equatorial climate system (Ramage, 1968). It lies beneath a zone of deep convection associated with the ascending branch of the Walker circulation (Tokinaga et al., 2012). Rainfall over the region range from 1,500 to 3,000 mm/year and the water balance is influenced by moisture convergence, monsoon circulation, and, to a lesser extent, continental recycling (Qian, 2008). Differential heating between oceanic and continental surface during the day drives land-sea breezes and enhances atmospheric convergence, which results in high insular precipitation (Neale & Slingo, 2003; Qian, 2008; Yamanaka, 2016). Rapid nocturnal land cooling shifts precipitation seaward and rainfall intensity weakens (Qian, 2008).

The Sunda shelf, which partially lies today 50 m below sea level, has been exposed (Figure 1b) during periods of glacial sea level stand (e.g., Voris, 2001). Moreover, geodynamics modified the long-term physiography of the shelf (Zahirovic et al., 2016), and likely permanently exposed the shelf prior to 400,000 years ago, regardless of sea level oscillations (Sarr et al., 2019). It is thus pivotal to constrain the climatic impact of the emerged Sunda shelf under interglacial conditions, such as present-day. Theoretically, exposing the shelf modifies convection and rainfall patterns simply through changes in thermal heat capacity and albedo, but more complex mechanisms involve changes in turbulent fluxes and dynamic processes that are specific of the Maritime Continent location in the monsoon/Walker circulation region. Exposing the shelf could also modify the pattern of the Indonesian Throughflow (ITF) by switching off the Karimata strait outflow.

The processes invoked in earlier modeling studies that focused on the impact of the Sunda shelf are contrasted (Bush & Fairbanks, 2003; Di Nezio et al., 2016; DiNezio & Tierney, 2013). Using both forced and fully coupled climate CESM1.0 simulations, Di Nezio et al. (2016) found that the Sunda shelf had a small impact when compared to the southern Sahul shelf, whereas an earlier study (Bush & Fairbanks, 2003) suggested that warming over the shelf enhanced convection and ultimately reinforced the Walker circulation. Possible reasons for these diverging results could involve (i) differential responses of rainfall to cloud radiative forcing (Stevens & Bony, 2013), (ii) differences in planetary boundary layer parameterization that can impact low-level circulation and convection (Shin et al., 2009), or (iii) differences in convection schemes (Gianotti et al., 2012).

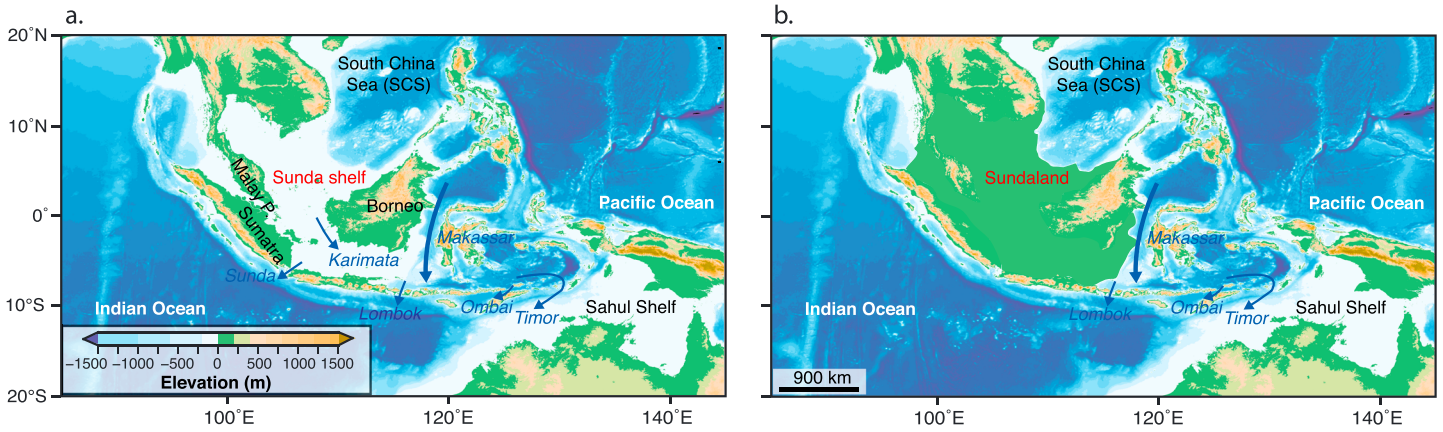

Figure 1. Topography and bathymetry of the Maritime Continent. (a) Present day. Light blue areas are the shallow Sunda and Sahul shelves that are emerged during periods of low-sea level (Voris, 2001). (b) With an emerged Sunda shelf. Arrows delineate the main passages of the South China Sea (SCS) and Indonesian Throughflow (ITF).

Our main objective is to quantify the effect of the Sunda shelf exposure on atmosphere and ocean dynamics, using in the first place a methodology comparable to that of Di Nezio et al. (2016) and Bush and Fairbanks (2003), besides the fact that we focus on the mechanisms triggering regional climate changes, in particular the chain reaction linking the effects of vegetation cover, atmospheric dynamics, and ocean freshwater budget. In this paper we also discuss (i) the differences among this and the aforementioned studies and (ii) the sensitivity of the shelf effect to the physical parameterization using an original set of simulations differing by their atmospheric physics and their convection schemes, as described in the following section.

2. Models and Experiments

2.1. Model Description

2.1.1. Atmospheric and Land Surface Models

In order to investigate the impact of atmospheric parameterization on the simulated climate over the Maritime Continent, we designed a set of simulations with two versions of the LMDz atmospheric general circulation model (Hourdin et al., 2006; Hourdin et al., 2013; Rochetin et al., 2014) (Table 1). We employed LMDz5A and LMDz6, respectively, used for CMIP5 and the ongoing CMIP6 simulations, coupled to the ORganizing Carbon and Hydrology In Dynamic EcosystEms (ORCHIDEE) land-surface model (Krinner et al., 2005) and forced by fixed sea-surface temperatures (hereafter SST-forced simulations).

In LMDz5A, the vertical turbulent transport within the boundary layer is treated as a diffusion following the formulation of Laval et al. (1981). Two different convection schemes (see section 2.2) can be selected to

Table 1
Simulation IDs and Characteristics

Simulation	Model Configuration	Convection Scheme	Physics	Shelf
1. Preindustrial SST-forced simulations				
CTL_KE	LMDZOR (v5)	Emanuel	Standard	N
CTL_TI	LMDZOR (v5)	Tiedtke	Standard	N
CTL_KEup	LMDZOR (v6)	Updated Emanuel	New	N
2. Shelf SST-forced simulations				
SHELF_KE	LMDZOR (v5)	Emanuel	Standard	Y
SHELF_TI	LMDZOR (v5)	Tiedtke	Standard	Y
SHELF_KEup	LMDZOR (v6)	Updated Emanuel	New	Y
GRASS_KE	LMDZOR (v5)	Emanuel	Standard	Y
3. Fully coupled simulations				
CM_CTL	IPSL-CM5A2	Emanuel	Standard	N
CM_SHELF	IPSL-CM5A2	Emanuel	Standard	Y

represent the shallow and deep convection (Hourdin et al., 2006): Emanuel (Emanuel, 1991) or Tiedtke (Tiedtke, 1989). The Morcrette (1991) scheme is used for radiative transfer. The model is run at a spatial resolution of 3.75° in longitude and 1.875° in latitude, and 39 vertical layers (i.e., 96 × 95 × 39 grid points). The activation of the zoom function centered on SE Asia enables to obtain a horizontal resolution of about 140 km over the Maritime Continent.

LMDz6 is the atmospheric component of the upcoming IPSL-CM6 model. In this version, implemented with the "New Physics" (Hourdin et al., 2015) parameterizations, the boundary layer representation relies on a combination of eddy diffusion (Yamada, 1983) and mass-flux representation of the organized thermal structure of the boundary layer (i.e., the thermal plume model; Rio & Hourdin, 2008). The longwave radiative transfer is based on the Rapid Radiation Transfer Model (Mlawer et al., 1997). The convection is based on an Emanuel scheme (Emanuel, 1991) that has been updated regarding to LMDz5 (see section 2.2). This version is run with a spatial resolution of 2.5° in longitude and 1.27° in latitude, and 79 vertical layers (144 × 142 × 79).

The land surface model ORCHIDEE (ORganizing Carbon and Hydrology In Dynamic EcosystEms; Krinner et al., 2005) simulates both biophysical and biochemical processes. Vegetation is represented by 13 plant functional types (PFTs) including bare soil. Albedo, surface roughness length, heat capacity, and leaf area index (LAI) are computed dynamically based on PFT phenologies. Evaporation efficiency is also computed; it depends on (i) the resistance between the canopy leaves and canopy top (so-called architectural resistance that affects transpiration), (ii) the bulk stomatal and leaves aerodynamical resistances (canopy resistance) that is inversely proportional to LAI and affects the evaporation of foliage water, and (iii) the drag coefficient that is inversely proportional to roughness. Runoff water is directed to the nearest ocean grid point.

At first order, LMDz simulates the regional pattern of rainfall realistically (Figure 2), although some biases, whose sign and amplitude depend on convection scheme (section 2.2), are depicted (see details in Text S1 and Figure S1). Rainfall seasonality is reproduce satisfactorily south of the equator, while the rainfall seasons start to early and precipitation amount is generally overestimated compared to observations northward of the equator (see details in Text S1 and Figure S2).

2.1.2. The Fully Coupled Model

Coupled simulations were performed with the ESM IPSL-CM5A2-VLR, which is the fast-computing derivative version of the IPSL-CM5A-LR model that was used for CMIP5 (Dufresne et al., 2013). This configuration benefits from an optimized hybrid parallelization, which improved the required computing time for coupled simulations (~75 versus 8 modeled year/day with IPSL-CM5A). This version also overcomes the global surface air temperature cold bias of IPSL-CM5A. Atmospheric and land surface models are, respectively, the LMDz5A and ORCHIDEE models described above. In addition, ocean is simulated by the ocean model NEMO (v3.6), with the ORCA2.3 configuration (Madec, 2016) that uses a global tripolar grid (two poles in the northern hemisphere to avoid singularity; Madec & Imbard, 1996) with a curvilinear mesh. This configuration has a resolution of 2° × 2°, refined at about 0.5° in the equatorial area, and 31 vertical levels (182 × 149 × 31) whose thicknesses increase from 10 m near the surface to 500 m at the bottom. IPSL-CM5A2 also includes the model LIM2 for sea ice thermodynamics (Fichefet & Maqueda, 1997). The atmosphere, ocean, land-surface, and sea ice components are linked via the OASIS coupler (Valcke et al., 2012).

As IPSL-CM5A, IPSL-CM5A2 has a wet bias over the Indo-Pacific tropical region when compared to observations (Dufresne et al., 2013). Whereas precipitations are overestimated over the ocean, some dry biases are found inland Borneo and Sumatra. Both biases have been described in most of CMIP5 (coupled) and AMIP5 (forced) models and are likely linked to systematic global circulation and monsoon biases (Toh et al., 2018). Sea surface salinity (SSS) pattern is realistic, with fresher condition inside the Indonesian archipelago with respect to the surrounding oceans (e.g., Gordon et al., 2003), but the model underestimates the salinity in the South China and Java Seas in relation with the rainfall positive bias.

2.2. Convection and Cloud Parameterization

Emanuel's and Tiedtke's convection schemes represent both the deep and the shallow convection. They are based on a "mass flux" approach and have their own cloud parameterization. In the Tiedtke scheme only one convective cloud, with a single saturated updraft, is considered. Entrainment and detrainment between cloud and environment can take place at any level between free convection level and free sinking level. Also,

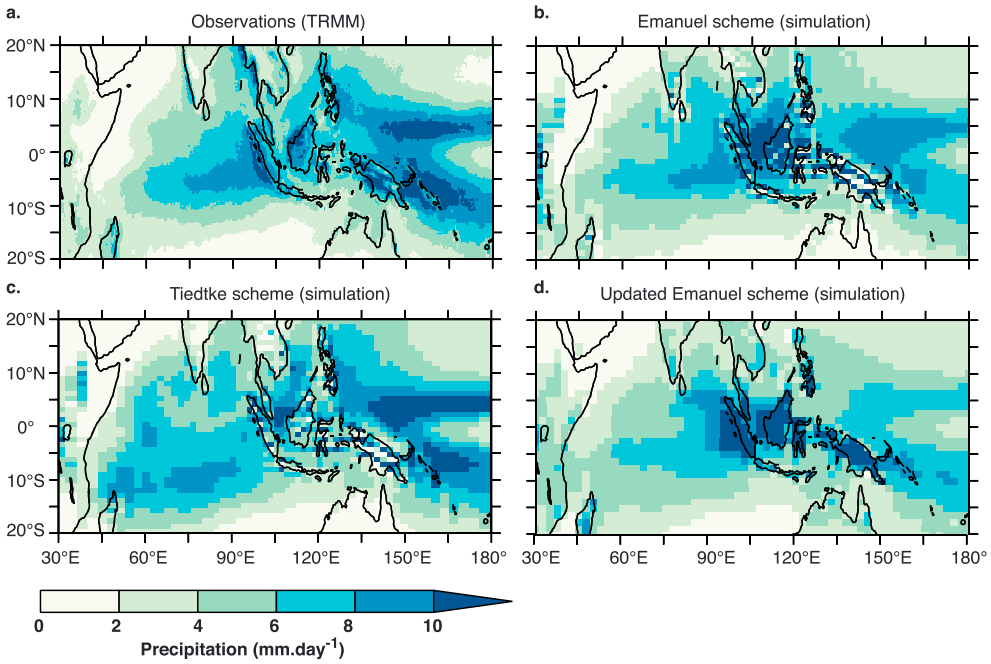

Figure 2. (a) Annual mean precipitation in TRMM (1979–2012) (Hilburn & Wentz, 2008). Simulated annual mean precipitation simulation for different convection scheme. (b) Emanuel scheme. (c) Tiedtke scheme. (d) Updated Emanuel scheme. Absolute values are plotted at initial data resolution while anomalies have been regridded on IPSL-CM5A2 simulation grid. Comparison with GPCP dataset (Huffmann et al., 2009) is provide as supporting information (Figure S1).

one single downdraft is considered, extending from the free sinking level to the cloud base, and assumed to be saturated and kept at saturation by evaporating precipitation. Mass flux at the top of the downdraft is directly proportional to updraft mass flux. Convection closure relies on moisture convergence and triggering is based on lifted parcel buoyancy in the first grid level above the condensation level. Homogeneous cloud fraction is calculated from the base to the top of the cloud and depends on the moist tendency simulated by the Tiedtke scheme.

The Emanuel scheme (Emanuel, 1991) considers convective fluxes based on an idealized model of subcloud-scale updrafts and downdrafts. The scheme assumes mixing within clouds to be highly episodic and inhomogeneous. The mixed updrafts move adiabatically up or down to their levels of neutral buoyancy while producing precipitation. In addition, a single downdraft is parameterized as a single entraining plume of constant fractional area driven by evaporation and precipitation. Both convection closure and triggering take into account tropospheric instability and convection inhibition. Mass flux at the cloud base relies on the convective available potential energy (CAPE). The convective cloud fraction calculation is based on the statistic distribution of total in-cloud water content following Bony and Emanuel (2001). Emanuel scheme is known to overestimate precipitation both over ocean and continent (Davis et al., 2009) while Tiedtke scheme overestimates precipitation over ocean at the cost of continental precipitation (see Figure 2, Figure S1, and Text S1 for details). Regarding the development history of LMDz, the shift from Tiedtke to Emanuel scheme allowed to improve the annual rainfall pattern of precipitation over the western part of the Indian Ocean (Braconnot et al., 2007; Hourdin et al., 2006).

In LMDz6, the Emanuel scheme has been updated to include the control of convection activation and intensity by subcloud processes. The convective closure (that determines the convective mass flux at the cloud base) and the triggering rely on the notion of Available Lifting Energy, which must overcome the convective inhibition, and Available Lifting Power that control convection power. Statistical lifting energy at the cloud base and convection triggering are based on a stochastic approach that relies on the properties of the thermal distribution characteristics (Rochetin et al., 2014). This version of the model has also improved representation of clouds. These updates of the convection scheme enable to improve the simulation of diurnal cycle in the tropics compared to former version of LMDz.

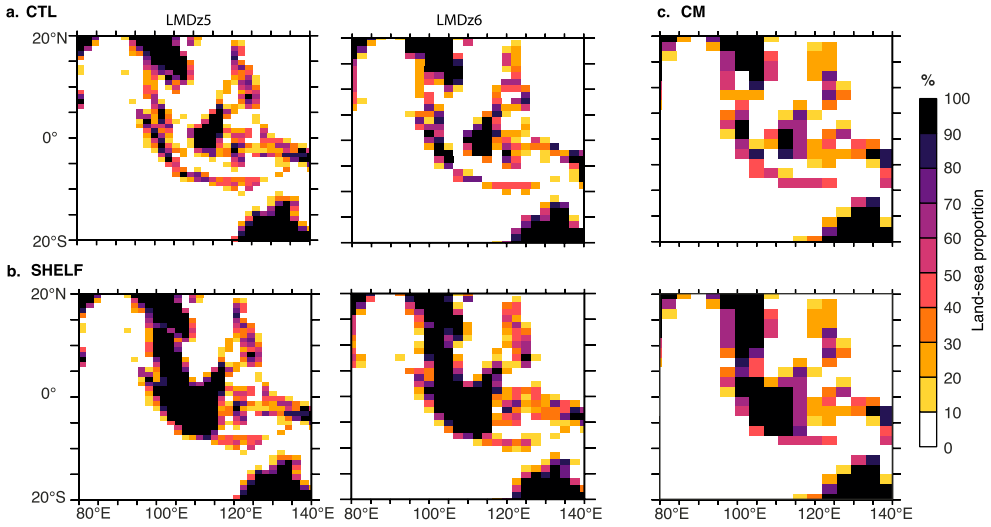

Figure 3. Land-sea masks. (a) CTL simulations. (b) SHELF simulations. (c) CM (coupled model) simulations.

2.3. Experimental Setup

We designed three different sets of simulations (Table 1). The first two sets are made of SST-fixed experiments with LMDz coupled to ORCHIDEE (hereafter LMDZOR configuration) and are used to explore the impact of parameterizations on simulated rainfall patterns over the Maritime Continent, the impact of the emerged shelf, and the influence of the prescribed vegetation. They are forced with fixed sea surface temperatures (AMIP II BCS Pseudo Sea Surface Temperature 1988–2007). The last set consists of two simulations run with the coupled IPSL-CM5A2 model, and is used to address the consequences of the shelf emergence on ocean dynamics.

2.3.1. Preindustrial SST-Forced Simulations

The first set of SST-forced simulations (CTL; Figure 3a) is made of experiments that have preindustrial boundary conditions (greenhouse gases concentration, ice sheet, bathymetry, sea surface temperature, insolation). Three different experiments have been performed with these boundary conditions: the first one uses LMDz5A with the Emanuel convection scheme and associated cloud scheme (CTL_KE), the second uses LMDz5A with Tiedtke convection scheme and associated cloud scheme (CTL_TI), and the last one uses LMDz6 with the updated Emanuel convection scheme (CTL_KEup) (Table 1). In CTL_TI and CTL_KE simulations we used the zoom function of the LMDz5A model (×2) to obtain a resolution of 0.9° to 1.95° in the Maritime Continent region. For CTL_KEup simulation we use the standard resolution of LMDz6 model which is to 2.5 by 1.27° over the Maritime Continent region. Those simulations were run for 30 years and we computed monthly and seasonal means over the last 20 years, using the 10 first years for spin-up.

2.3.2. Shelf SST-Forced Simulations

The second set of simulations was performed using the same model configurations, except that we modified the current land-sea mask by imposing the emersion of the Sunda Shelf, creating a continental area of 1.8×10^6 km^2 between Western Indonesian Islands and mainland South-East Asia (SHELF; Figure 3b), while other boundary conditions were kept as preindustrial. Vegetation over the platform was prescribed as 70% of tropical broad-leaved evergreen PFT and 30% of tropical broad-leaved raingreen PFT, following the current cover of neighboring areas. Four simulations have been performed with those boundary conditions (Table 1): three of them use the different convection and cloud parameterizations described above (SHELF_TI, SHELF_KE, and SHELF_KEup) and an additional one was run with the Emanuel's convection scheme (LMDz5A) and identical conditions, except for vegetation cover, that was set to 100% C4 grassland (GRASS_KE). Those two types of vegetation cover display different properties (albedo, roughness length, canopy water-holding capacity) that may influence surface-atmosphere coupling, hence the simulated surface climate (e.g., Davin & de Noblet-Ducoudré, 2010), via radiative and nonradiative processes.

2.3.3. Fully Coupled Simulations

A third set of simulations was run with IPSL-CM5A2 (Figure 3c, Table 1) to explore the impact of the shelf on the coupled ocean–atmosphere system. We used Emanuel's convection scheme and associated cloud scheme only, since the coupled model had been tuned with this scheme. We used a fully equilibrated, multimillenial preindustrial run (CM_CTL) from which we started an experiment (CM_SHELF) with an exposed shelf covered by a vegetation composed of 70% tropical broad-leaved evergreen PFT and 30% of tropical broad-leaved raingreen PFT. CM_SHELF has been run for 2,000 years and climatologies for both simulations were computed over the last 100 years.

3. Effect of Atmospheric Physics and Parameterization Scheme on Atmospheric Response Over the Maritime Continent

3.1. Impacts of Prescribed Physics on Annual and Seasonal Rainfall Simulated Changes

Figure 4a shows the change in precipitation between SHELF and CTL simulations for the three model configurations. In the KE configuration, shelf exposure results in higher annual mean precipitation over the Sunda shelf with amplitudes reaching +7 mm/day at the center of the shelf (Figure 4a, top). In the KEup configuration, shelf exposure results in higher annual mean precipitation over the central Sunda shelf, while precipitation decreases over Borneo and the eastern part of the Maritime Continent. The amplitude of the anomaly varies from +5 to −5 mm/day (Figure 4a, bottom). Conversely, using the Tiedtke scheme (SHELF_TI) leads to a decrease in mean annual precipitation over the shelf when it is emerged, a result that is comparable to what has been simulated in Di Nezio et al. (2016). Precipitation changes range from −4 to −1 mm/day and are mostly located on the northern part of the shelf.

Although with different amplitudes, all three configurations show that between 8°S and the equator, the shelf induces an increase in rainfall seasonal cycle, with higher precipitation rates during the transitional rainy seasons, that is, January–April and August–November (Figure 4b). KE and KEup configurations show almost no changes in precipitation during the boreal summer at these latitudes while TI simulates a strong drying (up to 5 mm/day) from May to August over this area, and a later drying between 2°N and 12°N from July to December. This negative mean annual precipitation changes simulated by Tiedtke convection scheme is due to inherent property of this scheme to overestimate year-round maritime rainfall at the cost of inland precipitation; when replacing ocean surfaces with continents, the Tiedtke's moisture advection bias mentioned earlier (section 2.2 and Text S1) is suppressed, leading to a decrease in convective activity and associated rainfall amount.

The seasonal increase in precipitation is associated to a general increase in low-level convergence on the exposed shelf, as pictured by near-surface wind divergence anomalies between SHELF_KE and CTL_KE for March–April season (Figures 5a and 5b). In turn moisture transport/advection from the Indian Ocean (Figure 5b) increases the water content of the tropospheric column, which favors both convective and stratiform precipitations (+3 mm/day; Table 2 and supporting information). These processes act during seasons of maximal insolation, namely, spring (Figure 5) and autumn equinoxes.

3.2. Mechanisms Driving the Shelf Effect on the Maritime Continent Rainfall

In the following, we analyze the daily outputs to explain the seasonal changes in precipitation when the shelf is exposed, only for the KE configurations, for the mechanism that triggers the increase in precipitations is similar in all the configurations (Figures S4 and S5). The 3-hr frequency fields (Figure 6) reveal higher variations of surface temperatures during the diurnal cycle of shelf surface over the shelf than over the ocean (SHELF_KE versus CTL_KE; Figure 6a). It results from the smaller heat capacity of the continental surface that allows for more efficient heat transfer when exposed to solar radiations. Whereas the diurnal amplitude of the near-surface temperature is low (~0.7 °C) in CTL_KE (Figure 6a), the exposed shelf reaches higher maximum temperatures at midday (+2 °C when compared to CTL_KE) and cools down rapidly (−2.8 °C when compared to CTL_KE) when insolation decreases (Figure 6a). The daily abrupt warming triggers the onset of convection, as shown by higher midlevel vertical velocity (>150 hPa/day; Figures 6b and 6c) and convective rainfalls (Figure 6d) that mimic the diurnal temperature cycle when the shelf is exposed (Figure 6a). Importantly, the daily averaged surface temperature is overall lower when the shelf is exposed, which explain why convection increases while the daily-averaged near-surface temperature decreases (Figure 6e).

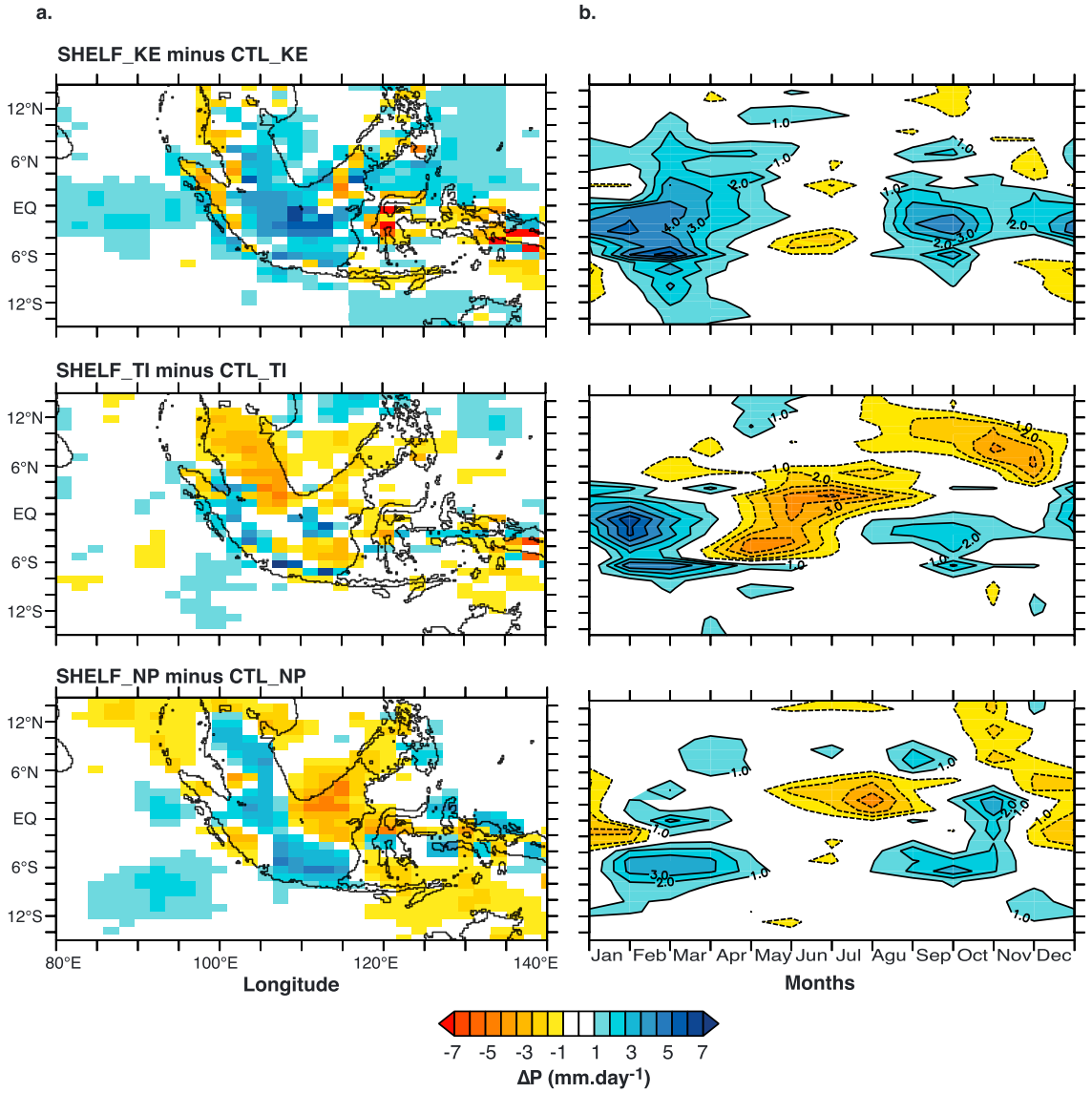

Figure 4. (a) Annual change in precipitation for LMDZOR simulation. (b) Hovmöller diagram showing the simulated change in seasonal precipitation along latitude (averaged over 95°E–115°E). (*top line*) SHELF_KE minus CTL_KE, (*middle*) SHELF_TI minus CTL_TI, and (*bottom line*) SHELF_KEup minus CTL_KEup. Dotted red line represents the limit between two different regimes of precipitation (e.g.,. Aldrian & Susanto, 2003).

Another consequence of surface heating is intensified moisture advection from the Indian Ocean (Figures 5b and S3), which releases more latent heat through condensation and stimulates convection. Enhanced moisture advection also induces higher specific humidity in the atmospheric column over the shelf. Figure 6d shows that a direct consequence is a permanent higher stratiform precipitation rate all over the day. Intensity of precipitation changes in transitional season appears to be directly related to vertical velocity when the shelf is emerged (Figures 6, S4, and S5).

4. Impact of Vegetation Cover on the Regional Climate

In this section we use the SST-forced configuration to explore the impact of vegetation cover on the platform and examine the radiative and turbulent fluxes budgets to understand the differences between SHELF_KE and GRASS_KE (Figure S6). In addition to the effect of surface heat capacity, replacing seawater with a vegetated shelf alters surface and air temperatures through changes in radiative balance and turbulent fluxes (equation (1) in the supporting information; Polcher et al., 1998). In SHELF_KE, the exposed shelf

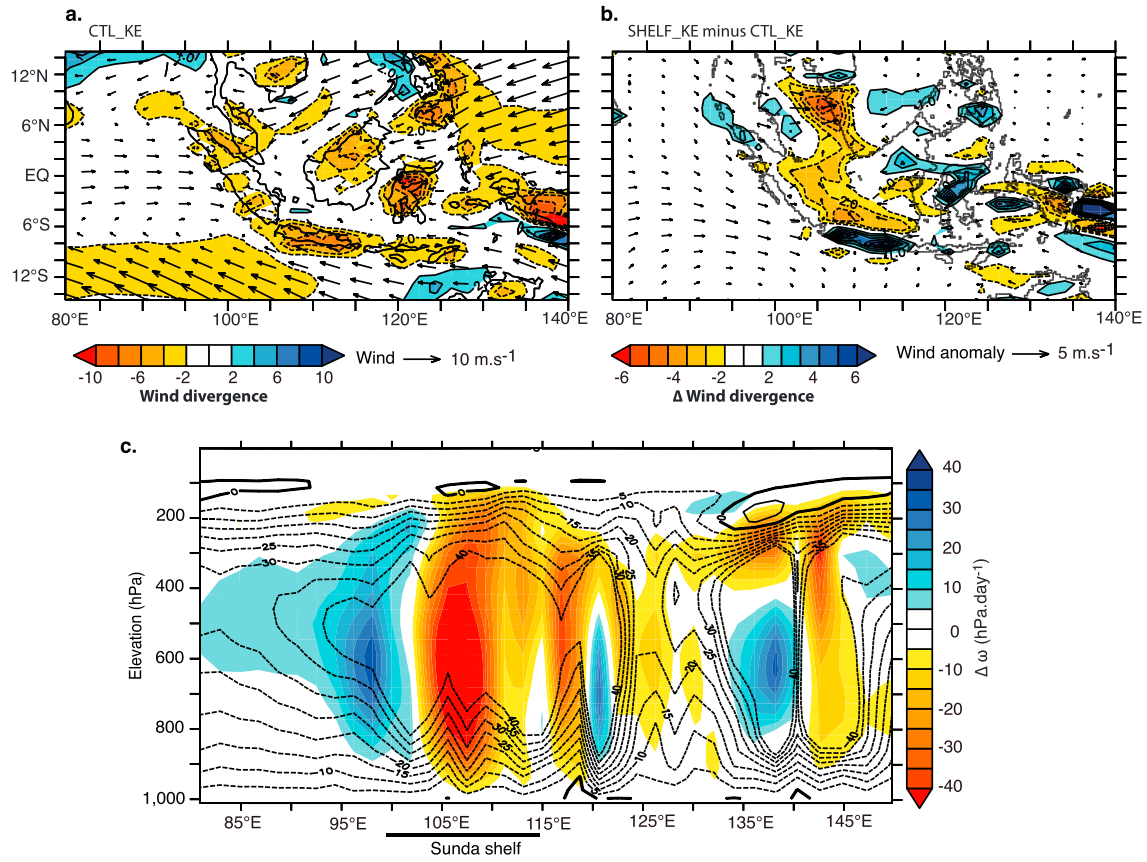

Figure 5. (a) Low-level divergence for CTL_KE simulation (with arrows for wind). (b) Change in low-level divergence (SHELF_KE minus CTL_KE, with arrows for wind anomaly). (c) Vertical wind anomalies (SHELF_KE minus CTL_KE; color-coded) and vertical wind component for CTL (dashed lines), averaged over 5°S–5°N latitudes and between March and April.

increases the yearly averaged surface albedo by 6% (Figure 7a and Table 2), thereby reducing the amount of absorbed short-wave radiations by −17.4 W/m^2. Given that lower LAI of herbaceous PFT, GRASS_KE simulation yields higher albedo (+8% compared to CTL_KE), and the net shortwave balance is thus reduced by 19 W/m^2. Still, average surface cooling is more pronounced in SHELF_KE (−1.9 °C) than in GRASS_KE (−0.8 °C; Table 2), showing the competing effect of albedo and nonradiative forcings. Turbulent fluxes act on the surface temperature through the energetic transfer from the surface to the boundary layer via sensible and latent heat. In our model, these fluxes are dependent on vegetation height (thus roughness; Figure 7b) and wind velocity that are expressed as the aerodynamic resistance (equation (4) in the supporting information). Sensible heat flux is controlled by the temperature gradient between surface and overlying atmosphere and by the aerodynamic resistance (equation (3) in the supporting information). When compared to CTL_KE, the higher roughness length (z_0) of the tree-covered surface in SHELF_KE are responsible for an increase in the sensible heat flux (H) by +10 W/m^2, which contributes to surface cooling. H in GRASS_KE is higher than in SHELF_KE (Figure S6), despite higher aerodynamic resistance, because of the competing effects of warmer surface and lower z_0.

Prescribing vegetation also has direct consequences on the latent heat flux (LE) through changes in evaporation. LE encompasses the effect of soil evaporation, canopy transpiration, and evaporation of foliage water (i.e., evaporation of rainfall water intercepted by the leaves, also called interception loss; equation (5) in the supporting information). The efficiency of each of these processes relies on water vapor pressure gradients and surface drag. With high LAI and z_0 over the shelf, SHELF_KE simulation depicts stronger evaporative rates and higher latent heat release than over adjacent ocean (+9 W/m^2). It ultimately increases surface cooling when compared to CTL_KE. In GRASS_KE, because of lower LAI and z_0, evaporation through interception loss is lower than in SHELF_KE, and thus, the total simulated latent heat flux at surface is lower

Table 2
Annual Change in Radiative and Turbulent Fluxes, and Surface Properties for FOREST and GRASS With Respect to CTL Simulation

	CTL	ΔSHELF_KE	ΔGRASS_KE
z_0	0.0004	1.6[a]	0.09[a]
αsurf	0.08	+0.06	+0.08
αTOA	0.26	+0.03	+0.04
SW↓ (W/m^2)	237.9	−4.3	−0.5
SW↑ (W/m^2)	18.7	+13.1	+19.0
Net SW (W/m^2)	219.3	−17.4	−19.5
LW↓ (W/m^2)	406.9	+2.4	+2.7
LW↑ (W/m^2)	467.4	−11.6	−4.6
Net LW (W/m^2)	−60.5	+14.0	+7.3
Rn (W/m^2)	155.1	−0.8	−7.6
H (W/m^2)	15.8	+10.5	+11.4
LE (W/m^2)	112.9	+13.5	+4.3
Tnsurf (°C)	26.7	−0.5	+0.03
Tsol (°C)	28.1	−1.9	−0.8
Total precipitation (mm/day)	10.	+2.3	+1.3
Drag	0.0013	−0.018	−0.003

Note. Parameter z_0 (roughness length) is given as an absolute value; α is the albedo; SW and LW are given, respectively, for shortwave and longwave radiations (W/m^2); Rn is the radiative budget (W/m^2); *H* is the sensible heat flux (W/m^2); LE is the latent heat flux (W/m^2); and Tsurf and Tsol are, respectively, the near-surface temperature and the surface temperature (°C).
[a]The z_0 parameter is given as absolute value for the consider surface. All other number in those two columns are differences.

(−11.6 W/m^2), despite higher transpiration rate. This smaller loss of energy through LE release compensates the albedo effect and produces a lower surface cooling in GRASS_KE than in SHELF_KE.

5. Oceanic Response

Here we use the fully coupled simulations to explore the impact of simulated change in precipitation on ocean as well as atmosphere–ocean feedback. CM_SHELF experiment accounts for the ocean–atmosphere coupling and yields a similar response to shelf exposure than SHELF_KE experiment (Figures S7 and S8), which suggests rather weak ocean–atmosphere feedback. Significant increase in seasonal rainfall and year-round decrease of mean surface temperature are simulated over the Maritime Continent (Figure S8). Although of lower magnitude, a significant increase in convergence and convection over the shelf is simulated during the maximum insolation season (Figure S7). Increased convergence drives a small increase in total cloud cover and convective precipitation (up to +1 mm/day) over the eastern Indian Ocean south of the equator, but these changes have no significant consequences for the more global (i.e., tropical Indian and Pacific) ocean dynamics. No significant changes in SST, wind stress, or thermocline depth are simulated over this region.

Conversely, the emergence of the Sunda shelf directly re-routes water masses and changes in continental freshwater inputs, which modifies

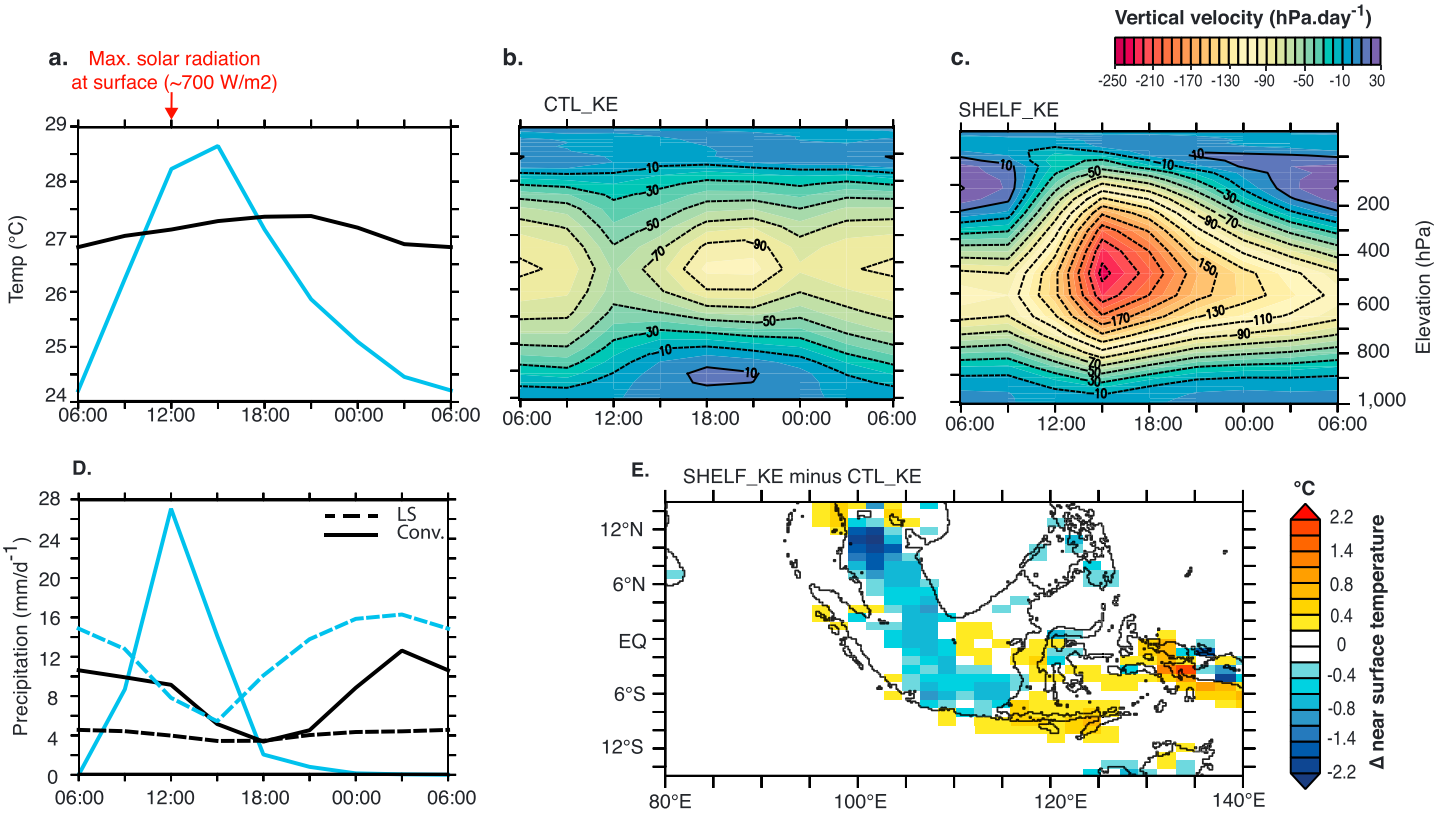

Figure 6. The 3-hr frequency field (annually averaged) of (a) near-surface temperature, vertical velocity ((b) CTL_KE and (c) SHELF_KE), and (d) precipitation averaged over a 105°E–108°E and 2°S–2°N box. Blue and black curves are, respectively, the SHELF_KE and CTL_KE simulations. (e) Annual mean change in near-surface temperature between SHELF_KE and CTL_KE.

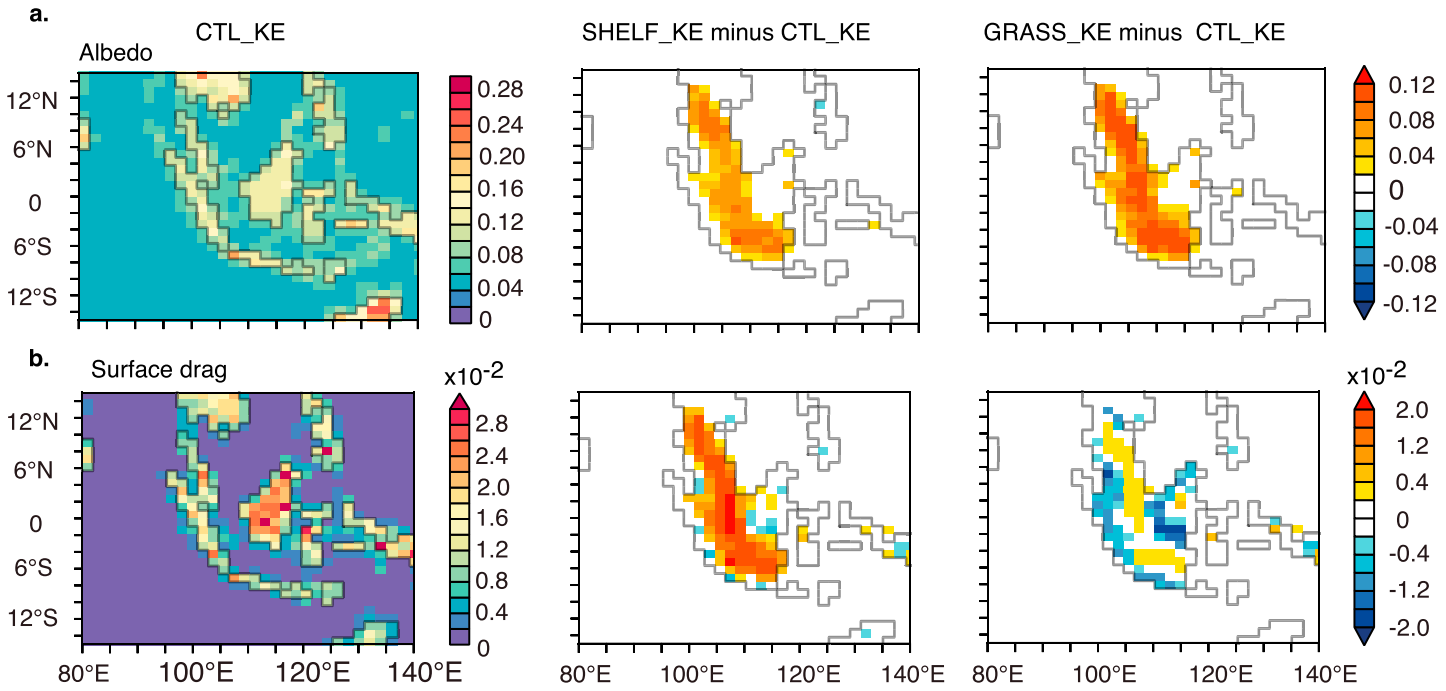

Figure 7. (*left*) Shelf surface properties for CTL simulation and change in surface properties (*middle*) between SHELF_KE and CTL_KE simulation and (*right*) GRASS_KE and CTL_KE simulation. (a) Albedo. (b) Neutral drag coefficient (function of the roughness length z_0).

the adjacent ocean temperature and salinity fields through direct re-routing of water masses and changes in continental freshwater inputs. First, emerging the Sunda shelf shuts off the Karimata strait (between Sumatra and Borneo; Figure 1), which in turn modifies the South China Sea (SCS) water export. Subtropical Pacific waters enter the SCS via Luzon strait, west of the Philippines. When the shelf is inundated, those waters are heated in the SCS and exported via the Karimata strait during boreal winter (Gordon et al., 2003). Consistent with previous results obtained with ocean-only models, wherein the SCS throughflow is switched off (Tozuka et al., 2009; Tozuka et al., 2015), our simulations show that the closure of the Karimata strait prevents this water export toward the Java Sea and ITF and results in increased SST in the SCS (up to +1.4 °C seasonally; Figure 8a). The closure of the SCSTF is also responsible for an increase in Makassar strait transport (Table S1).

Shutting down the seawater exchange between SCS and the ITF modifies the dynamics of the ITF, which alters both SST and SSS of water masses surrounding the shelf: in CM_SHELF simulation, the southward volume and heat advection in the Makassar strait increases (supporting information and Table 2), especially during boreal winter (1.4 Sv and 0.2 PW with a reference temperature of 0 °C), when the contribution of the SCS throughflow is the highest (Figure 8b). Increased heat export warms the tropical Indian Ocean (up to +1.2 °C) with maximum temperature anomalies located along the coasts of Sumatra and Java (Figure 7a), where SST annual variability is the highest (standard deviation is ~0.8°), as already found by Tozuka et al. (2009, 2015).

CM_SHELF also shows a significant increase in salinity in the ITF (~ +3 psu) and in the Banda Sea, while the salinity along West Sumatra coast decreases by ~1 psu (Figures 8b and 8c). The former signal is explained by two mechanisms: first, the lower rainfall simulated over the Makassar strait (Eastern Borneo) when the shelf is exposed mechanically displaces the local freshwater balance and leads to higher surface salinity. Second, closing the connection between SCS and ITF switches off the wind-driven southeastward export of relatively fresher water from SCS through the Karimata strait (Figure 8b; e.g., Gordon et al., 2003; Tozuka et al., 2009). Such results are in line with previous studies that show modified dynamics of the ITF due to the closure of the Karimata strait (Qu et al., 2006; Tozuka et al., 2007; Tozuka et al., 2009; Tozuka et al., 2015). Paleoproxy data also indicate higher salinity in the ITF during the last glacial maximum, when the Sunda shelf was emerged, which is explained by a reinforced input of high-salinity water

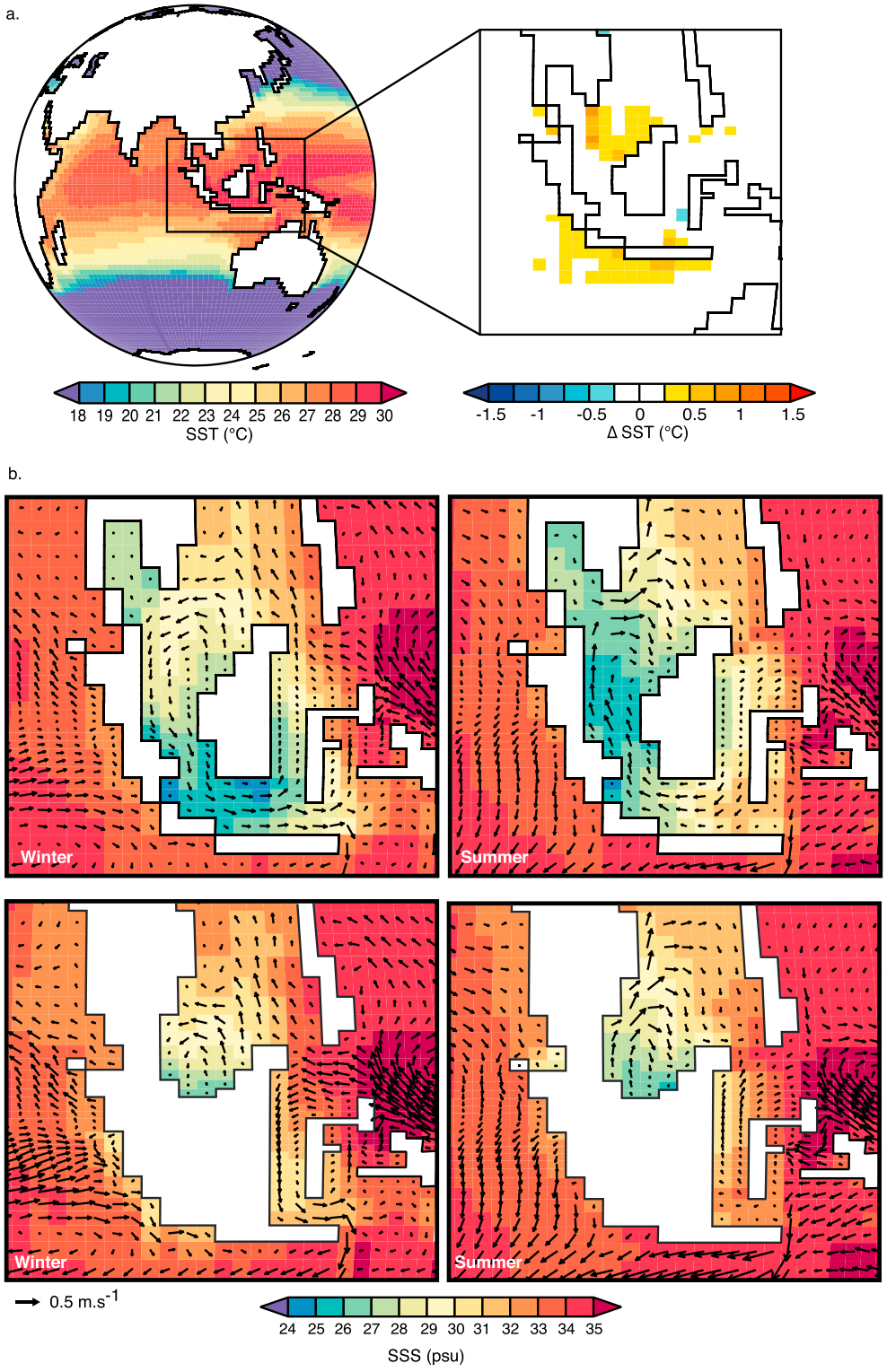

Figure 8. (a, *left*) Annually averaged sea surface temperature and (*right*) change in SST (CM_SHELF minus CM_CTL). (b) Seasonal SSS (shaded areas) and sea surface currents in the ITF. (*top*) CM_CTL, (*bottom*) CM_SHELF, (left) winter (JFMA), and (*right*) summer (JJAS).

from the tropical Pacific Ocean (Martinez et al., 2002) and a lower *P-E* balance associated with enhanced evaporation in the ITF (De Deckker et al., 2003). The simulated increased SSS in the ITF appears to be a rather robust result, while the large magnitude may be related to underestimation of Java Sea salinity in the CTL simulation.

Changes in SSS over the eastern Indian Ocean are indirect consequences of rainfall changes over the emerged shelf. Increased rainfall leads to substantial amounts of continental runoff and associated freshwater coastal flow off the shelf. As a consequence of this freshwater input, the nearshore SSS decreases by up to 2.5 psu offshore west of Sumatra (Figure 8c).

A detailed assessment of these changes on large-scale climate variability, namely, El Niño–Southern Oscillation patterns, was beyond our scope, but preliminary analysis shows little to no influence of the shelf on ENSO patterns.

6. Discussion

6.1. General Mechanism by Which the Sunda Shelf Alter the Regional Climate

Our results suggest that an emerged Sunda shelf induces a regional climatic response characterized by seasonal enhancement of moisture convergence and continental precipitation driven by the thermal properties of the land surface. Changes in temperature linked to shelf emergence result from the combined effects of continental heat capacity, surface albedo, and turbulent fluxes. The simulated surface cooling mainly results from the lower thermal inertia of land compared to ocean, which leads to a strong diurnal cycle of temperature over the shelf. On seasonal average, we find that the surface cooling amplitude results from the competing effect of surface albedo change and turbulent fluxes; these two mechanisms depend on vegetation characteristics, including roughness length and evaporative capacity over foliage. Such competing roles of radiative and nonradiative forcings have been described in earlier studies focusing on deforestation (Davin & de Noblet-Ducoudré, 2010; Port et al., 2016). The amplitudes of moistening of the regional climate also depend on the vegetation type, with higher precipitation when a forested shelf is prescribed.

6.2. Impact of Parameterizations on the Results

In this study, the simulated increase in convective activity with the emerged shelf is in line with the hypotheses of Dayem et al. (2007) and Molnar and Cronin (2015), who suggest that convection scales with the size of the Maritime Continent. Bush and Fairbanks (2003) also predict an enhanced convection and higher rainfall rates over the shelf. Di Nezio et al. (2016) also simulated surface cooling, but found that it induced lower convection and drying of the shelf. Di Nezio et al. (2016) used the CESM model, whose convection scheme relies on Richter and Rasch (2008) for the deep convection and Park and Bretherton (2009) for the shallow convection. These two schemes have been shown to produce lower precipitation rates in the convective area of the Maritime Continent when compared to Emanuel's (Toh et al., 2018). In the light of our sensitivity tests, we suggest that discrepancies among previous studies and our results regarding the shelf influence on rainfall patterns likely arise from differing parameterizations as well. Still, although the annual simulated rainfall response to shelf emergence depends on the modeling frameworks used, the mechanism linking shelf exposure to enhanced convergence and convection is retrieved in all studies, while the seasonal increase in convection appears independent of the convection scheme. We therefore contend that the enhanced convective effect of the Sunda shelf is robust.

6.3. Spatial Resolution as a Caveat for Quantifying the Shelf Impact?

The spatial resolution used in our numerical experiments prevent a full representation of land-sea breezes process over the Maritime Continent, as suggested in earlier studies (Qian, 2008). Yet the alternative not only resides in an improved resolution: models with increased spatial resolution yield rather contrasted results. Schiemann et al. (2014) have run sensitivity experiments with the HadGAM1 AGCM, downscaling the grid spacing from about 350 to about 110 km (a comparable resolution to our SST-forced simulations). They show that the increased resolution indeed improved rainfall patterns in the tropics, and that this improvement was linked to a better representation of land details and fractional land-sea mask. More importantly, they suggested that the sensitivity of precipitation to resolution over the Maritime Continent was reduced for further increase in resolution (namely, 60-km resolution), whereas it involved significant

changes and constraints to ensure numerical stability, such as reducing the physical time steps. These results have been confirmed by Johnson et al. (2016), who also added that deficiencies in parameterizations may become more apparent at high resolution, because many GCM parameterizations were originally designed for low resolution. Other models, either regional circulation model (Li et al., 2017) or AGCMs (CAM model (Bacmeister et al., 2014)), corroborate these results. Love et al. (2011) show that parameterized convection tends to misrepresent the diurnal cycle of precipitation. They therefore suggest that only very high resolution (4 km) configurations, explicitly resolving convection, could correct precipitation biases, but in turn also created systematic wet biases due to the difficulties of conserving moisture in the semi-Lagrangian conservation scheme.

Here our aim is to quantify climate changes linked to the shelf emergence by means of sensitivity experiments involving both SST-forced and fully coupled experiments. LMDz simulations do not explicit a dry bias, and the shelf-induced increase in advection leading to higher precipitation over the region appears as a robust signal among the different simulations. Setting up very high resolution numerical experiments would likely reduce our model biases for present-day simulations, but would unlikely provide different results in terms of Sunda shelf influence on climate, given the mechanisms at stake.

6.4. Ocean Impact and Perspectives

We find that the shelf alters sea surface salinity through both direct and indirect effects. Higher precipitation rates over the exposed platform induce freshwater discharge to adjacent ocean and thus lower surface salinity. The salinity budget in the present-day ITF is impacted both by local precipitation-evaporation balance and freshwater input via the SCS (Gordon et al., 2003). During periods of shelf emergence, the removal of freshwater input from the SCS may be partly compensated by continental runoff, which emphasizes the importance of past river routing reconstruction to understand paleoclimatic changes in the region. In our experiment, continental runoff over the shelf is routed toward the closest ocean grid points via coastal flow, with no prescribed river transport. An early reconstruction of the exposed platform (Molengraaff, 1921) described a large river network with outlets both in SCS and ITF. Increasing precipitation over the platform should impact the water fluxes in such large river systems and further impact may be recorded in circulation and stratification of the ITF. The interpretation of ocean paleoproxies should account for this change in freshwater budget conditions. A more comprehensive understanding of the impact of an emerged Sunda shelf on the regional ocean dynamics would also benefit from a better resolved ocean that would permit to explicitly represent fluxes through narrow straits like Ombai or Lombok.

Unfortunately, no direct comparison of our results with proxies is feasible to date, since published paleoclimatic indicators in the region focus on the last glacial maximum and the Holocene. Last glacial maximum conditions involve lower atmospheric CO_2 concentration, larger ice sheets, and an emerged Sahul shelf, all of which having potential impact on tropical climate dynamics (e.g., Di Nezio et al., 2016), while the Sunda shelf was already drowned during the Holocene. Nonetheless, future works focusing on past interglacial periods should consider the impacts of an exposed Sunda shelf.

Acknowledgments
This work was granted access to the HPC resources of TGCC under the allocation 2018-A0030102212 made by GENCI. We would like to thank Frédéric Hourdin and Pascale Braconnot for their discussions. We are grateful to two anonymous reviewers that help in improving the manuscript. Inputs files necessary to reproduce experiments are available upon request (anta.clarisse.sarr@gmail.com). The model output is archived at https://vesg.ipsl.upmc.fr/thredds/catalog/store/sarrac/SarretalJGR/catalog.html.

References

Aldrian, E., & Susanto, R. D. (2003). Identification of three dominant rainfall regions within Indonesia and their relationship to sea surface temperature. *International Journal of Climatology*, *23*(12), 1435–1452. https://doi.org/10.1002/joc.950

Bacmeister, J. T., Wehner, M. F., Neale, R. B., Gettelman, A., Hannay, C., Lauritzen, P. H., et al. (2014). Exploratory high-resolution climate simulations using the Community Atmosphere Model (CAM). *Journal of Climate*, *27*(9), 3073–3099. https://doi.org/10.1175/JCLI-D-13-00387.1

Bony, S., & Emanuel, K. A. (2001). A Parameterization of the Cloudiness Associated with Cumulus Convection; Evaluation Using TOGA COARE Data. *Journal of the Atmospheric Sciences*, *58*, 3158–3183. https://doi.org/10.1175/1520-0469(2001)058<3158:APOTCA>2.0.CO;2

Braconnot, P., Hourdin, F., Bony, S., Dufresne, J.-L., Grandpeix, J.-Y., & Marti, O. (2007). Impact of different convective cloud schemes on the simulation of the tropical seasonal cycle in a coupled ocean–atmosphere model. *Climate Dynamics*, *29*(5), 501–520. https://doi.org/10.1007/s00382-007-0244-y

Bush, A. B., & Fairbanks, R. G. (2003). Exposing the sunda shelf: Tropical responses to eustatic sea level change. *Journal of Geophysical Research*, *108*(D15), 4446. https://doi.org/10.1029/2002JD003027

Davin, E. L., & de Noblet-Ducoudré, N. (2010). Climatic impact of global-scale deforestation: Radiative versus non-radiative processes. *Journal of Climate*, *23*(1), 97–112. https://doi.org/10.1175/2009JCLI3102.1

Davis, N., Bowden, J., Semazzi, F., Xie, L., & Onol, B. (2009). Customization of RegCM3 regional climate model for eastern Africa and a tropical Indian Ocean domain. *Journal of Climate*, *22*(13), 3595–3616. https://doi.org/10.1175/2009JCLI2388.1

Dayem, K. E., Noone, D. C., & Molnar, P. (2007). Tropical western Pacific warm pool and Maritime Continent precipitation rates and their contrasting relationships with the Walker circulation. *Journal of Geophysical Research*, *112*, D06101. https://doi.org/10.1029/2006JD007870

de Deckker, P., Tapper, N., & van der Kaars, S. (2003). The status of the Indo-Pacific warm pool and adjacent land at the last glacial maximum. *Global and Planetary Change*, *35*(1–2), 25–35. https://doi.org/10.1016/S0921-8181(02)00089-9

DiNezio, P. N., & Tierney, J. E. (2013). The effect of sea level on glacial Indo-Pacific climate. *Nature Geoscience*, *6*(6), 485–491. https://doi.org/10.1038/ngeo1823

Di Nezio, P., Timmermann, A., Tierney, J. E., Jin, F.-F., Otto-Bliesner, B., Rosenbloom, N., et al. (2016). The climate response of the indo-pacific warm pool to glacial sea level. *Paleoceanography*, *31*, 866–894. https://doi.org/10.1002/2015PA002890

Dufresne, J.-L., Foujols, M.-A., Denvil, S., Caubel, A., Marti, O., Aumont, O., et al. (2013). Climate change projections using the IPSL-CM5 Earth system model: From CMIP3 to CMIP5. *Climate Dynamics*, *40*(9–10), 2123–2165. https://doi.org/10.1007/s00382-012-1636-1

Emanuel, K. A. (1991). A scheme for representing cumulus convection in large-scale models. *Journal of the Atmospheric Sciences*, *48*(21), 2313–2329. https://doi.org/10.1175/1520-0469(1991)048<2313:ASFRCC>2.0.CO;2

Fichefet, T., & Maqueda, M. (1997). Sensitivity of a global sea ice model to the treatment of ice thermodynamics and dynamics. *Journal of Geophysical Research*, *102*(C6), 12,609–12,646. https://doi.org/10.1029/97JC00480

Gianotti, R. L., Zhang, D., & Eltahir, E. A. (2012). Assessment of the regional climate model version 3 over the maritime continent using different cumulus parameterization and land surface schemes. *Journal of Climate*, *25*(2), 638–656. https://doi.org/10.1175/JCLI-D-11-00025.1

Gordon, A. L., Susanto, R. D., & Vranes, K. (2003). Cool Indonesian Throughflow as a consequence of restricted surface layer flow. *Nature*, *425*(6960), 824–828. https://doi.org/10.1038/nature02038

Hilburn, K. A., & Wentz, F. J. (2008). Intercalibrated passive microwave rain products from the Unified Microwave Ocean Retrieval Algorithm (UMORA). *Journal of Applied Meteorology and Climatology*, *47*(3), 778–794. https://doi.org/10.1175/2007JAMC1635.1

Hourdin, F., Foujols, M.-A., Codron, F., Guemas, V., Dufresne, J.-L., Bony, S., et al. (2013). Impact of the LMDz atmospheric grid configuration on the climate and sensitivity of the IPSL-CM5A coupled model. *Climate Dynamics*, *40*(9–10), 2167–2192. https://doi.org/10.1007/s00382-012-1411-3

Hourdin, F., Gueye, M., Diallo, B., Dufresne, J. L., Escribano, J., Menut, L., et al. (2015). Parameterization of convective transport in the boundary layer and its impact on the representation of the diurnal cycle of wind and dust emissions. *Atmospheric Chemistry and Physics*, *15*, 6775–6788. https://doi.org/10.5194/acp-15-6775-2015

Hourdin, F., Musat, I., Bony, S., Braconnot, P., Codron, F., Dufresne, J.-L., et al. (2006). The LMDz4 general circulation model: Climate performance and sensitivity to parameterized physics with emphasis on tropical convection. *Climate Dynamics*, *27*(7–8), 787–813. https://doi.org/10.1007/s00382-006-0158-0

Huffman, G. J., Adler, R. F., Bolvin, D. T., & Gu, G. (2009). Improving the global precipitation record: GPCP version 2.1. *Geophysical Research Letters*, *36*, L170808. https://doi.org/10.1029/2009GL040000

Johnson, S. J., Levine, R. C., Turner, A. G., Martin, G. M., Woolnough, S. J., Schiemann, R., et al. (2016). The resolution sensitivity of the South Asian monsoon and Indo-Pacific in a global 0.35° AGCM. *Climate Dynamics*, *46*, 807–831. https://doi.org/10.1007/s00382-015-2614-1

Krinner, G., Viovy, N., de Noblet-Ducoudré, N., Ogée, J., Polcher, J., Friedlingstein, P., et al. (2005). A dynamic global vegetation model for studies of the coupled atmosphere-biosphere system. *Global Biogeochemical Cycles*, *19*, GB1015. https://doi.org/10.1029/2003GB002199

Laval, K., Sadourny, R., & Serafini, Y. (1981). Land surface processes in a simplified general circulation model. *Geophysical & Astrophysical Fluid Dynamics*, *17*, 129–150. https://doi.org/10.1080/03091928108243677

Li, Y., Jourdain, N. C., Taschetto, A. S., Gupta, A. S., Argüeso, D., Masson, S., & Cai, W. (2017). Resolution dependence of the simulated precipitation and diurnal cycle over the Maritime Continent. *Climate Dynamics*, *48*(11–12), 4009–4028. https://doi.org/10.1007/s00382-016-3317-y

Love, B. S., Adrian, J. M., & Grenville, M. S. L. (2011). The diurnal cycle of precipitation over the Maritime Continent in a high-resolution atmospheric model. *Quarterly Journal of the Royal Meteorological Society*, *137*(657), 934–947. https://doi.org/10.1002/qj.809

Madec, G., & Imbard, M. (1996). A global ocean mesh to overcome the north pole singularity. *Climate Dynamics*, *12*(6), 381–388. https://doi.org/10.1007/BF00211684

Madec, G., & the NEMO team (2016). Nemo ocean engine. Ocean Dynamic Component: NEMO–OPA, Note du Pôle de modélisation de l'Institut Pierre-Simon Laplace No 27.

Martinez, J. I., De Deckker, P., & Barrows, T. T. (2002). Palaeoceanography of the Western Pacific Warm Pool during the last glacial maximum: Long-term climatic monitoring of the Maritime Continent. In P. Kershaw, B. David, N. Tapper, D. Penny, & J. Brown (Eds.), *Bridging Wallace s Line, Advances in Geoecology* (Vol. 34, pp. 147–172). Reiskirchen, Germany: Catena Verlag.

Mlawer, E. J., Taubman, S. J., Brown, P. D., Iacono, M. J., & Clough, S. A. (1997). Radiative transfer for inhomogeneous atmospheres: RRTM, a validated correlated-*k* model for the longwave. *Journal of Geophysical Research*, *102*(D14), 16,663–16,682. https://doi.org/10.1029/97JD00237

Molengraaff, G. (1921). Modern deep-sea research in the East Indian archipelago. *The Geographical Journal*, *57*(2), 95–118. https://doi.org/10.2307/1781559

Molnar, P., & Cronin, T. W. (2015). Growth of the maritime continent and its possible contribution to recurring ice ages. *Paleoceanography*, *30*, 196–225. https://doi.org/10.1002/2014PA002752

Morcrette, J.-J. (1991). Radiation and cloud radiative properties in the European Centre for Medium Range Weather Forecasts forecasting system. *Journal of Geophysical Research*, *96*(D5), 9121–9132. https://doi.org/10.1029/89JD01597

Neale, R., & Slingo, J. (2003). The maritime continent and its role in the global climate: A GCM study. *Journal of Climate*, *16*(5), 834–848. https://doi.org/10.1175/1520-0442(2003)016<0834:TMCAIR>2.0.CO;2

Park, S., & Bretherton, C. S. (2009). The University of Washington shallow convection and moist turbulence schemes and their impact on climate simulations with the Community Atmosphere Model. *Journal of Climate*, *22*(12), 3449–3469. https://doi.org/10.1175/2008JCLI2557.1

Polcher, J., McAvaney, B., Viterbo, P., Gaertner, M.-A., Hahmann, A., Mahfouf, J.-F., et al. (1998). A proposal for a general interface between land surface schemes and general circulation models. *Global and Planetary Change*, *19*(1-4), 261–276. https://doi.org/10.1016/S0921-8181(98)00052-6

Port, U., Claussen, M., & Brovkin, V. (2016). Radiative forcing and feedback by forests in warm climates—A sensitivity study. *Earth System Dynamics*, *7*(3), 535–547. https://doi.org/10.5194/esd-7-535-2016

Qian, J.-H. (2008). Why precipitation is mostly concentrated over islands in the maritime continent. *Journal of the Atmospheric Sciences*, *65*(4), 1428–1441. https://doi.org/10.1175/2007JAS2422.1

Qu, T., Du, Y., & Sasaki, H. (2006). South China Sea throughflow: A heat and freshwater conveyor. *Geophysical Research Letters*, *33*, L23617. https://doi.org/10.1029/2006GL028350

Ramage, C. S. (1968). Role of a tropical "Maritime Continent" in the atmospheric circulation. *Monthly Weather Review*, *96*(6), 365–370. https://doi.org/10.1175/1520-0493(1968)096<0365:ROATMC>2.0.CO;2

Richter, J. H., & Rasch, P. J. (2008). Effects of convective momentum transport on the atmospheric circulation in the Community Atmosphere Model, version 3. *Journal of Climate*, *21*(7), 1487–1499. https://doi.org/10.1175/2007JCLI1789.1

Rio, C., & Hourdin, F. (2008). A thermal plume model for the convective boundary layer: Representation of cumulus clouds. *Journal of the Atmospheric Sciences*, *65*(2), 407–425. https://doi.org/10.1175/2007JAS2256.1

Rochetin, N., Grandpeix, J. Y., Rio, C., & Couvreux, F. (2014). Deep convection triggering by boundary layer thermals. Part II: Stochastic triggering parameterization for the LMDZ GCM. *Journal of the Atmospheric Sciences*, *71*(2), 515–538. https://doi.org/10.1175/JAS-D-12-0337.1

Sarr, A.-C., Husson, L., Sepulchre, P., Pastier, A.-M., Pedoja, K., Elliot, M., et al. (2019). Subsiding Sundaland. *Geology*, *47*(2), 119–122. https://doi.org/10.1130/G45629.1

Schiemann, R., Demory, M.-E., Mizielinski, M. S., Roberts, M. J., Shaffrey, L. C., Strachan, J., & Vidale, P. L. (2014). The sensitivity of the tropical circulation and Maritime Continent precipitation to climate model resolution. *Climate Dynamics*, *42*(9-10), 2455–2468. https://doi.org/10.1007/s00382-013-1997-0

Shin, S.-H., Kimoto, M., Ha, K.-J., & Yun, K.-S. (2009). Impact of different diffusion schemes on simulated rainfall: Land-ocean contrast. *Journal of Geophysical Research*, *114*(D13), D13101. https://doi.org/10.1029/2008JD011605

Stevens, B., & Bony, S. (2013). What are climate models missing ? *Science*, *340*(6136), 1053–1054. https://doi.org/10.1126/science.1237554

Tiedtke, M. (1989). A comprehensive mass flux scheme for cumulus parameterization in large-scale models. *Monthly Weather Review*, *117*, 1179–1800.

Toh, Y. Y., Turner, A. G., Johnson, S. J., & Holloway, C. E. (2018). Maritime Continent seasonal climate biases in AMIP experiments of the CMIP5 multimodel ensemble. *Climate Dynamics*, *50*(3–4), 777–800. https://doi.org/10.1007/s00382-017-3641-x

Tokinaga, H., Xie, S.-P., Deser, C., Kosaka, Y., & Okumura, Y. M. (2012). Slowdown of the Walker circulation driven by tropical Indo-Pacific warming. *Nature*, *491*(7424), 439. https://doi.org/10.1038/nature11576–443.

Tozuka, T., Qu, T., Masumoto, Y., & Yamagata, T. (2009). Impacts of the South China Sea throughflow on seasonal and interannual variations of the Indonesian Throughflow. *Dy- namics of Atmospheres and Oceans*, *47*(1–3), 73–85. https://doi.org/10.1016/j.dynatmoce.2008.09.001

Tozuka, T., Qu, T., & Yamagata, T. (2007). Dramatic impact of the South China Sea on the Indonesian Throughflow. *Geophysical Research Letters*, *34*, L12612. https://doi.org/10.1029/2007GL030420

Tozuka, T., Qu, T., & Yamagata, T. (2015). Impacts of South China Sea throughflow on the mean state and El Niño/Southern Oscillation as revealed by a coupled GCM. *Journal of Oceanography*, *71*(1), 105–114. https://doi.org/10.1007/s10872-014-0265-1

Valcke, S., Balaji, V., Craig, A., DeLuca, C., Dunlap, R., Ford, R., et al. (2012). Coupling technologies for Earth system modelling. *Geoscientific Model Development*, *5*(6), 1589–1596. https://doi.org/10.5194/gmd-5-1589-2012

Voris, H. K. (2001). Maps of Pleistocene sea levels in Southeast Asia: Shorelines, river systems and time durations. *Journal of Biogeography*, *27*(5), 1153–1167. https://doi.org/10.1046/j.1365-2699.2000.00489.x

Yamada, T. (1983). Simulations of Nocturnal Drainage Flows by a q2l Turbulence Closure Model. *Journal of the Atmospheric Sciences*, *40*, 91–106. https://doi.org/10.1175/1520-0469(1983)040<0091:SONDFB>2.0.CO;2

Yamanaka, M. D. (2016). Physical climatology of Indonesian maritime continent: An outline to comprehend observational studies. *Atmospheric Research*, *178–179*, 231–259. https://doi.org/10.1016/j.atmosres.2016.03.017

Zahirovic, S., Flament, N., Müller, D. R., Seton, M., & Gurnis, M. (2016). Large fluctuations of shallow seas in low-lying Southeast Asia driven by mantle flow. *Geochemistry, Geophysics, Geosystems*, *17*, 3589–3601. https://doi.org/10.1002/2016GC006434